Prog. Theor. Phys. Suppl. 138, 543 - 548 (2000)

Morphological characterization of spatial patterns

K. Michielsen[1*)], H. De Raedt[2**)] and J.G.E.M. Fraaije[1 ***)]

[1]*Laboratory for Biophysical Chemistry*
[2]*Institute for Theoretical Physics and Materials Science Centre*
University of Groningen, Nijenborgh 4
NL-9747 AG Groningen, The Netherlands

(Received)

We describe a morphological image analysis method to characterize spatial patterns in terms of geometry and topology. This involves the calculation of the Minkowski functionals and the analysis of these functionals as a function of control parameters. The method is applied to triply periodic minimal surfaces and to three-dimensional structures formed in polymer solutions.

§1. Introduction

Geometrical patterns are encountered in many different fields of science and technology, including porous media, biology, polymer chemistry, metallography, geology and astronomy.[1),2)] We characterize these patterns in terms of shape (geometry) and connectivity (topology) by means of morphological image analysis (MIA). This involves the calculation of the Minkowski functionals known from integral geometry.[3),4)] These functionals are related to familiar measures: In two (three) dimensions they correspond to the covered area, boundary length, and connectivity (volume, surface area, integral mean curvature and connectivity) of the pattern. For sufficiently smooth and regular objects some of these measures are related to quantities known from differential geometry. Integral geometry imposes no limitations on the properties of the patterns. Furthermore in integral geometry the calculation of the Minkowski functionals is relatively straightforward and requires little computational effort.[22)]

Given a set of patterns the first step in MIA is to compute the Minkowski functionals themselves. The second step is to analyze the behavior of the Minkowski functionals as a function of control parameters. This approach has proven to be instrumental to describe the morphology of porous media and complex fluids, the large-scale distribution of matter in the Universe, microemulsions, patterns in reaction diffusion systems, and spinodal decomposition kinetics.[5)]

In this paper we briefly discuss the underlying mathematics of the Minkowski

*) E-mail: K.F.L.Michielsen@chem.rug.nl
**) E-mail: deraedt@phys.rug.nl
***) E-mail: J.G.E.M.Fraaije@chem.rug.nl

functionals and the algorithm to compute them. We illustrate the application of MIA to three-dimensional (3D) patterns taken from polymer chemistry and to minimal surfaces.

§2. Minkowski functionals

We consider the convex ring $\mathcal{R}$, which is the class of all subsets A of $\mathbb{R}^d$ which can be expressed as finite unions of compact convex sets $A = \cup_{i=1}^n K_i$ with $K_i \in \mathbb{K}$, the class of all compact convex sets. If A_1 and A_2 both belong to $\mathcal{R}$ then so do $A_1 \cup A_2$ and $A_1 \cap A_2$. An additive functional φ on $\mathcal{R}$ has the properties $\varphi(\emptyset) = 0$ and $\varphi(A_1 \cup A_2) = \varphi(A_1) + \varphi(A_2) - \varphi(A_1 \cap A_2)$ for A_1, $A_2 \in \mathcal{R}$. Motion invariance of φ on $\mathcal{R}$ is defined as follows: $\varphi(gK) = \varphi(K)$ if $K \in \mathbb{K}$ and g is a translation or rotation in $\mathbb{R}^d$. An important additive and motion invariant functional on $\mathcal{R}$ is the Euler characteristic χ. For $K \in \mathbb{K}$, $\chi(K) = 1$ if $K \neq \emptyset$ and $\chi(K) = 0$ if $K = \emptyset$. For finite unions of compact convex sets the additivity property leads to

$$\chi(A) = \chi\left(\cup_{i=1}^n K_i\right) = \sum_i \chi(K_i) - \sum_{i<j} \chi(K_i \cap K_j) + \ldots + (-1)^{n+1} \chi(K_1 \cap \ldots \cap K_n). \tag{1}$$

The value of $\chi(A)$ is independent of the representation of A as a finite union of compact convex sets.[3] The functional χ can be shown to agree with the Euler characteristic as defined in algebraic topology.[3] Very often one is interested in the topology of a surface.[2] Its Euler characteristic is associated with the surface ∂A of A. $\chi(A)$ is related to $\chi(\partial A)$ by $\chi(\partial A) = \chi(A)[1 - (-1)^n]$, where n is the dimension of the body K ($n \leq d$).[6]

The Euler characteristic provides a starting point to define the Minkowski functionals $W_\nu^{(d)}(A)$ for $A \in \mathcal{R}$[3]

$$\begin{aligned} W_\nu^{(d)}(A) &= \int \chi(A \cap E_\nu) d\mu(E_\nu) \qquad \nu = 0, \ldots, d-1, \\ W_d^{(d)}(A) &= \omega_d \chi(A) \qquad \omega_d = \pi^{d/2} / \Gamma(1 + d/2), \end{aligned} \tag{2}$$

where E_ν is a ν-dimensional plane in $\mathbb{R}^d$ and $d\mu(E_\nu)$ denotes its motion-invariant kinematical density[3] normalized so that for a d-dimensional ball $B_d(r)$ with radius r, $W_\nu^{(d)}(B_d(r)) = \omega_d r^{d-\nu}$ with ω_d the volume of the unit ball,[5] with the convention $\omega_0 = 1$. The Minkowski functionals inherit from χ the property of additivity (see (1)) and motion invariance. These features together with their "conditional continuity" ($W_\nu^{(d)}$ are continuous when restricted to $\mathbb{K}$) specify the Minkowski functionals as morphological measures, i.e. as a family of geometrical and topological descriptors.[5] In three dimensions we have: $W_0 = V$, $W_1 = S/3$, $W_2 = H/3$ and $W_3 = 4\pi\chi/3$, where V denotes the volume, S the surface area and H the integral mean curvature. An important result in integral geometry is the completeness of the family of Minkowski functionals. A theorem by Hadwiger[3] states that every motion-invariant, additive and conditionally continuous functional can be written as a linear combination of the Minkowski functionals with suitable real coefficients.

In order to analyze images on a computer we first have to digitize them.[7] The digitization process requires the mapping of the image on a grid and a quantization of the gray level. We will consider 3D images partitioned into cubes. Each cube is centered at a lattice point and is called a voxel. In general the range of gray levels is divided into bins and the gray level at any lattice point is required to take on only one of these values. We reduce the gray-scale images to black-and-white pictures by thresholding. If the given picture $\mathcal{P}(\mathbf{x})$ with $\mathbf{x} \in \mathbb{R}^d$ has gray level range $[a, b]$, and t is any number between a and b, the result of thresholding $\mathcal{P}(\mathbf{x}, t)$ at t is the two-valued picture $\mathcal{P}(\mathbf{x}, t)$ defined by[7] $\mathcal{P}(\mathbf{x}, t) = 1$ if $\mathcal{P}(\mathbf{x}, t) \geq t$ and $\mathcal{P}(\mathbf{x}, t) = 0$ if $\mathcal{P}(\mathbf{x}, t) < t$. We assign to $\mathcal{P}(\mathbf{x}, t) = 0$ a white voxel (the background) and to $\mathcal{P}(\mathbf{x}, t) = 1$ a black voxel (the object). Once the thresholded image is obtained it becomes possible to discuss the morphological properties of the picture subsets. As the 3D image is build up from white and black voxels and each voxel is a compact convex set, we may consider the image as a finite union of convex sets. For practical purposes we consider each voxel as the union of the disjoint collection of its interior, faces, open edges and vertices.[22] We first compute the Minkowski functionals for these single open structures. Then, by making use of the property of additivity of the Minkowski functionals and the fact that there is no overlap between open bodies on a lattice, we compute the Minkowski functionals for the whole pattern $\mathcal{P}(\mathbf{x}, t)$.[22]

§3. Triply periodic minimal surfaces

A minimal surface in $\mathbb{R}^3$ is defined as a surface for which the mean curvature is zero at each of its points. As a consequence, at every point of a minimal surface the two principal curvatures are equal, but opposite in sign. We will consider the triply periodic minimal surfaces (TPMS), minimal surfaces that are periodic in three independent directions. During the last years these TPMS and similar interfaces have been elaborately discussed in literature since structures related to TPMS may form spontaneously in physico-chemical and in biological systems.[2),8)] MIA allows to study the topology of TPMS without making use of labyrinth graphs or surface tiling.[18)]

Periodic surfaces can be divided into equivalent regions bounded by a unit cell of space. There are two common choices of unit cells, the lattice fundamental region and the crystallographic cell.[10)] We give our data for the crystallographic cell, simply called the unit cell from now on, and assume that the bicontinuous structure of total volume L^3 is composed of several unit cells of typical length scale L_0. Then the Euler characteristic χ of the whole system is given by $\chi = \overline{X}(L/L_0)^3 \equiv \overline{\chi}N$, where N denotes the number of unit cells. The volume, area and integral mean curvature of the whole system may be written as $V = \overline{V}L_0^3N$, $S = \overline{S}L_0^2N$, $B = \overline{B}L_0N$. The quantities $\overline{V}$, $\overline{S}$, $\overline{B}$ and $\overline{\chi}$ characterize the structure within one elementary unit cell. We compute the Minkowski functionals for the P (primitive)[11)] the D (diamond)[11)] and the G (gyroid)[12)] surfaces. These surfaces divide space into two equal labyrinths related by a translation (for P and D) or an inversion (for G), thereby generating a bicontinuous geometry. The labyrinths are of connectivity 6, 4 and 3 for the P, D and G surface respectively. The oriented P, D and G surfaces may be approximated

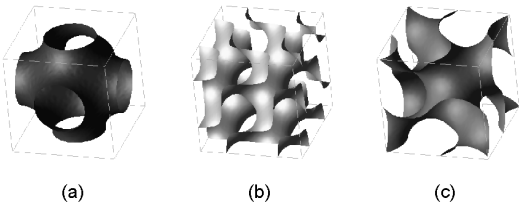

Fig. 1. Unit cube for the nodal primitive P surface (a), the nodal double diamond D surface (b) and the nodal gyroid G surface (c). The surfaces are generated from (3), (4) and (5).

by the periodic nodal surfaces [13) - 15)]

$$\cos x + \cos y + \cos z = 0 \tag{3}$$

$$\sin x \sin y \sin z + \sin x \cos y \cos z + \cos x \sin y \cos z + \cos x \cos y \sin z = 0 \tag{4}$$

$$\sin x \cos y + \sin y \cos z + \sin z \cos x = 0. \tag{5}$$

In Fig. 1 we show the nodal P, D and G surfaces, in their unit cell. Table 1 summarizes the geometrical properties for the thresholded nodal oriented P, D and G surfaces for one unit cell and $L_0 = 128$. The values for the geometrical properties, calculated using integral geometry based MIA, are in good agreement with the numbers quoted in literature. [10), 16), 17)] The numbers for the area are about a factor of 1.6 larger than the numbers quoted in literature. This systematic error is due to the thresholding of the picture. This operation transforms the smooth surface to a more stepwise surface which enlarges the covered area.

Table I. Morphological measures of the thresholded P, D and G surface ($t = 0.5$) obtained from (3), (4), (5) for $N = 1$ and $L_0 = 128$. The values found in the literature [10), 16), 17)] are given in brackets.

TPMS	$\overline{V}$	$\overline{S}$	$\overline{\chi}$
P	0.5 (0.5)	3.675 (2.345)	-2 (-2)
D	0.5 (0.5)	6.000 (3.838)	-8 (-8)
G	0.5 (0.5)	4.847 (2.093)	-4 (-4)

§4. Soft materials

In "soft materials", which exhibit both temporal and spatial structural fluctuations over many length and time scales, the underlying lattice is formed under certain thermodynamic conditions and is far less rigid than the lattice of atomic crystals. The application of conventional crystallographic techniques to identify the mesostructures in these "soft" materials may be rather difficult. As an example we calculate the Minkowski functionals and the structure factor for computer simulation data of a 50% aqueous solution of a triblock copolymer surfactant (ethylene oxide)$_{13}$(propylene oxide)$_{30}$ (ethylene oxide)$_{13}$ [or (EO)$_{13}$(PO)$_{30}$(EO)$_{13}$]. The data are generated with a 3D dynamic mean-field density functional method, [19)] a numerical method for the simulation of coarse-grained morphology dynamics in polymer liquids. The experimental [20)] and simulated [21)] phase diagram in the 50-70% surfactant concentration interval agree well and consist of four different phases: a micellar, an hexagonal, a bicontinuous and a lamellar phase. The inset in Fig.2 shows the morphology of propylene oxide in a 50% aqueous solution of (EO)$_{13}$(PO)$_{30}$(EO)$_{13}$ for a

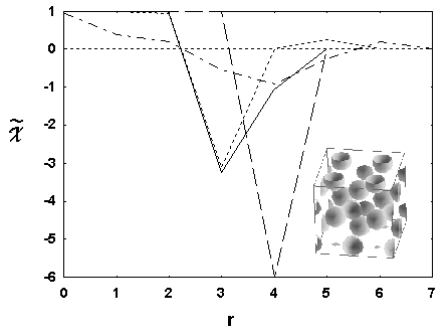

Fig. 2. Euler characteristic as a function of r. Solid line: simulation data of a 50% aqueous solution of $(EO)_{13}(PO)_{30}(EO)_{13}$ in a cubic box of edge length 16; dashed line: Perfect BCC lattice with $N = 2$ and $L_0 = 8$; dotted line: BCC lattice with $N = 2$ and $L_0 = 8$ and all lattice points displaced over a randomly chosen distance 0 or 1; dash-dotted line: Random set of 16 points in a cubic box of edge length 16. Inset: morphology of PO in a 50% aqueous solution of $(EO)_{13}(PO)_{30}(EO)_{13}$.

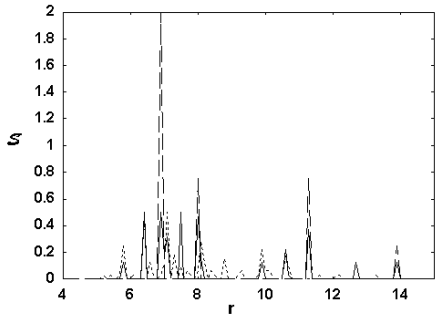

Fig. 3. Structure factor as a function of r. Solid line: simulation data of a 50% aqueous solution of $(EO)_{13}(PO)_{30}(EO)_{13}$ in a cubic box of edge length 16; dashed line: Perfect BCC lattice with $N = 2$ and $L_0 = 8$; dotted line: BCC lattice with $N = 2$ and $L_0 = 8$ and all lattice points displaced over a randomly chosen distance 0 or 1.

cubic simulation box of edge length 16 with periodic boundaries.

In order to study the Minkowski functionals for these polymer systems we first threshold the 3D image. Then we determine the centres (germs) of the micelles in the black and white picture and use the following graining procedure: We consider the germs to be spheres of radius $r = 0$. We enlarge the spheres by coloring black all voxels that are positioned at a distance smaller or equal to $r > 0$ from the germs. The grains form discrete approximations to spheres in $\mathbb{R}^d$.

In Fig.2 we depict the Euler characteristic $\widetilde{\chi} \equiv \chi/M$, where M denotes the number of germs, as a function of r for the polymer solution in the cubic simulation box of edge length 16 (solid line). The number of germs equals 16. For comparison we also show $\widetilde{\chi}$ for the perfect body-centered cubic (BCC) lattice with $L_0 = 8$ and $N = 2$ (dashed line), for the same BCC lattice but all lattice points displaced over a randomly chosen distance 0 or 1 (dotted line) and for a random set of 16 points in a cubic box of edge length 16 (dash-dotted line). From Fig.2 and the behavior of the other Minkowski functionals (not shown) we may conclude that the micelles are organized in a BCC lattice structure with $L_0 = 8$ and $N = 2$ and of which the lattice points are somewhat displaced. The Euler characteristic per unit cell for the micellar phase equals two, which is also characteristic for a BCC lattice structure. From the Euler characteristic $\widetilde{\chi}$ as a function of r we may see that the radius of the micelles has to be smaller than three lattice units. Otherwise the micelles glue together and $\widetilde{\chi}$ differs from one. Fig.3 demonstrates that it is much harder to draw a similar conclusion from the structure factor $\mathcal{S}(r)$ of the same system. The structure

factor for the polymer solution (solid line) does not resemble the structure factor for a BCC lattice with $L_0 = 8$ and $N = 2$ (dashed line), nor the structure factor for a BCC lattice structure with $L_0 = 8$ and $N = 2$ and of which the lattice points are somewhat displaced (dotted line). In a bigger simulation box (edge length 32) the micelles are no longer organized on a BCC lattice structure, neither their distribution is random, as can be concluded from the Minkowski functionals (results not shown). Again, the latter conclusion is difficult to draw from the structure factor.

§5. Summary

We have described a morphological image analysis (MIA) method to characterize spatial patterns in terms of shape (geometry) and connectivity (topology). Integral geometry based MIA allows a relatively straightforward calculation of the Minkowski functionals and requires little computational effort. The approach has been illustrated by computation of the morphological measures of triply periodic minimal surfaces and of complex structures formed in polymer solutions. In the latter case MIA provides information about the mesostructures that is hard to obtain by other methods.

Acknowledgements

We are grateful to Prof. H. Wagner for very helpful advice. We would like to thank G.J.A. Sevink for providing us the simulation data on the Pluronic-water mixtures. This work is partially supported by a SON-Unilever research contract.

References

1) P. Ball, *The Self-Made Tapestry: Pattern Formation in Nature* (Oxford University Press, 1998).
2) S. Hyde, S. Andersson, K. Larsson, Z. Blum, T. Landh, S. Lidin, B.W. Ninham, *The Language of Shape; The role of curvature in condensed matter: Physics, Chemistry and Biology* (Elsevier, Amsterdam, 1997).
3) H. Hadwiger, *Vorlesungen über Inhalt, Oberfläche und Isoperimetrie* (Springer Verlag, Berlin, 1957).
4) D. Stoyan, W.S. Kendall, J. Mecke, *Stochastic Geometry and its Applications* (Akademie Verlag, Berlin, 1989).
5) K.R. Mecke, Int. J. Mod. Phys. **B12** (1998), 861.
6) C.N. Likos, K.R. Mecke, H. Wagner J. Chem. Phys. **102** (1995), 9350.
7) A. Rosenfeld, A.C. Kak, *Digital Picture Processing*, (Academic Press, New York, 1982).
8) J. Klinowski, A.L. Mackay, H. Terrones, Phil. Trans. R. Soc. Lond. **A354** (1996), 1975.
9) W. Fischer, E. Koch, Z. Kristallog. **179** (1987), 31.
10) K. Grosse-Brauckmann, J. Coll. Interf. Sci. **187** (1997), 418.
11) H.A. Schwarz, *Gesammelte Mathematische Abhandlungen*, (Springer, Berlin, 1890).
12) A.H. Schoen, *Infinite periodic minimal surfaces without self-intersections*, NASA Technical NOTE No. D-5541 (1970).
13) A.L. Mackay, Proc. R. Soc. Lond. **A442** (1993), 47.
14) C.A. Lambert, L.H. Radzilowski, E.L. Thomas, Phil. Trans. R. Soc. Lond. **A354** (1996), 2009.
15) A. Ciach, R. Hołyst, J. Chem. Phys. **110** (1999), 3207.
16) W.T. Góźdź and R. Hołyst, Phys. Rev. **E54** (1996), 5012.
17) S.T. Hyde, Langmuir **13** (1997), 842.

18) W. Fischer, E. Koch, Act. Cryst. **A45** (1989), 726.
19) J.G.E.M. Fraaije, B.A.C. van Vlimmeren, N.M. Maurits, M. Postma, O.A. Evers, C. Hoffmann, P. Altevogt, G. Goldbeck-Wood, J. Chem. Phys. **106** (1997), 4260.
20) P. Alexandridis, U. Olsson, B. Lindmann, Macromolecules **28** (1995), 7700.
21) B.A.C. van Vlimmeren, N.M. Maurits, A.V. Zvelindovsky, G.J.A. Sevink, J.G.E.M. Fraaije, Macromolecules **32** (1999), 646.
22) K. Michielsen, H. De Raedt, J.G.E.M. Fraaije, preprint.